



High-Content Screening and Computational Prediction Reveal Viral Genes That Suppress the Innate Immune Response

Tai L. Ng,^{a,b} Erika J. Olson,^{a,b} Tae Yeon Yoo,^a H. Sloane Weiss,^{a,b} Yukiye Koide,^{a,b} Peter D. Koch,^{a,b} Nathan J. Rollins,^a Pia Mach,^{a,b} Tobias Meisinger,^a Trenton Bricken,^a Timothy Z. Chang,^{a,b} Colin Molloy,^{a,b} Jérôme Zürcher,^a Roger L. Chang,^{a,b} Timothy J. Mitchison,^a John I. Glass,^c Debora S. Marks,^a Jeffrey C. Way,^{a,b,d} Pamela A. Silver^{a,b,d}

^aDepartment of Systems Biology, Harvard Medical School, Boston, Massachusetts, USA

^bWyss Institute for Biologically Inspired Engineering, Harvard University, Boston, Massachusetts, USA

^cJ. Craig Venter Institute, La Jolla, California, USA

^dLaboratory of Systems Pharmacology, Harvard Medical School, Boston, Massachusetts, USA

ABSTRACT Suppression of the host innate immune response is a critical aspect of viral replication. Upon infection, viruses may introduce one or more proteins that inhibit key immune pathways, such as the type I interferon pathway. However, the ability to predict and evaluate viral protein bioactivity on targeted pathways remains challenging and is typically done on a single-virus or -gene basis. Here, we present a medium-throughput high-content cell-based assay to reveal the immunosuppressive effects of viral proteins. To test the predictive power of our approach, we developed a library of 800 genes encoding known, predicted, and uncharacterized human virus genes. We found that previously known immune suppressors from numerous viral families such as *Picornaviridae* and *Flaviviridae* recorded positive responses. These include a number of viral proteases for which we further confirmed that innate immune suppression depends on protease activity. A class of predicted inhibitors encoded by *Rhabdoviridae* viruses was demonstrated to block nuclear transport, and several previously uncharacterized proteins from uncultivated viruses were shown to inhibit nuclear transport of the transcription factors NF- κ B and interferon regulatory factor 3 (IRF3). We propose that this pathway-based assay, together with early sequencing, gene synthesis, and viral infection studies, could partly serve as the basis for rapid *in vitro* characterization of novel viral proteins.

IMPORTANCE Infectious diseases caused by viral pathogens exacerbate health care and economic burdens. Numerous viral biomolecules suppress the human innate immune system, enabling viruses to evade an immune response from the host. Despite our current understanding of viral replications and immune evasion, new viral proteins, including those encoded by uncultivated viruses or emerging viruses, are being unearthed at a rapid pace from large-scale sequencing and surveillance projects. The use of medium- and high-throughput functional assays to characterize immunosuppressive functions of viral proteins can advance our understanding of viral replication and possibly treatment of infections. In this study, we assembled a large viral-gene library from diverse viral families and developed a high-content assay to test for inhibition of innate immunity pathways. Our work expands the tools that can rapidly link sequence and protein function, representing a practical step toward early-stage evaluation of emerging and understudied viruses.

KEYWORDS expression systems, virus-host interactions

Pathogenic viruses (e.g., Ebola virus, HIV, severe acute respiratory syndrome coronavirus 2 [SARS-CoV-2]) continue to pose public health threats and cause economic disruptions worldwide. The human innate immune system has evolved multiple signaling pathways, including the type I interferon pathway, to defend against viral

Editor Ileana M. Cristea, Princeton University

Copyright © 2022 Ng et al. This is an open-access article distributed under the terms of the [Creative Commons Attribution 4.0 International license](https://creativecommons.org/licenses/by/4.0/).

Address correspondence to Pamela A. Silver, pamela_silver@hms.harvard.edu, or Jeffrey C. Way, pamela_silver@hms.harvard.edu.

The authors declare no conflict of interest.

Received 13 December 2021

Accepted 21 February 2022

Published 23 March 2022

infections. These pathways use nucleic acid receptors to trigger timely immune responses, including the expression of proteins that halt viral replication and production of interferon that activates the JAK/STAT signaling pathway (1, 2). Viruses have evolved several ways to evade these mechanisms, such as binding or degrading proteins in these pathways, molecular mimicry, or modulating host gene expression (3–6). Identifying viral proteins that block immune signaling leads to potential drug targets and a significantly improved understanding of viral replication.

Despite substantial progress in our knowledge of viral pathogenicity and immune evasion, a standardized and consistent study for rapidly investigating many different viruses remains underexplored due to challenges such as optimizing virus cultivation and defining cell type. Furthermore, next-generation sequencing and proteomics have provided an abundance of uncharacterized viral proteins, with many generically annotated as nonstructural proteins or hypothetical proteins (7). Even for functionally validated proteins, annotations inferred across species may prove to be inaccurate without experimental validations. Some viral enzymes, such as viral proteases, may have unidentified moonlighting roles as immune suppressors (8). The number of such uncharacterized sequences is expected to continue to grow massively from large-scale virus collection and surveillance projects (9). Altogether, these challenges limit our understanding of viral pathogenicity and, consequently, treatment of viral infections.

We envision a multipronged approach using a suite of assays that can rapidly identify different functions of unknown viral proteins. Such screens could complement viral infection studies pursued by academic labs or dedicated government facilities for viral surveillance. Ultimately, these assays will further extend our knowledge of immune evasion by viruses. We explored this concept by starting with the development of a medium-throughput, microscopy-based immune assay in BJ-5ta fibroblasts. We assembled a library of 605 genes from viruses belonging to 31 families, including 536 sequences with unannotated immunosuppressive function. We tested an additional 195 coronavirus genes during the coronavirus disease 2019 (COVID-19) pandemic. Our assay identified many inhibitors, some of which were previously reported, some with immunosuppressive function that was inferred from sequence similarity or Pfam homology, and some with unsuspected potential for immune suppression.

RESULTS

Viral gene library construction. First, we aimed to develop a library of viral genes that would further our understanding of human viruses (Fig. 1). We envisioned that our library should contain known immune inhibitors, homologues of immune inhibitors, and uncharacterized proteins. We also focused on human and insect host viruses to highlight relevance to diseases, as well as understudied viruses from diverse viral families. Six thousand protein sequences were collected from GenBank reference genomes of the 1,688 human viruses in VirusHostDB (10). To sample diverse proteins spanning this set, we clustered at >20% sequence identity and >80% coverage using CD-HIT (11, 12), resulting in 1,975 clusters. Well-conserved viral proteins such as capsids and replication enzymes were collected in large clusters of up to over 100 members, whereas hundreds of sequences had no close relatives in other reference genomes. To increase the chances of identifying immune suppressors, we focused on smaller genomes (<35 genes). We also excluded likely integral membrane proteins, as they may not properly fold in the absence of other viral proteins. We also excluded large polypeptides that are typically cleaved in the context of a viral infection.

To collect viral genes known and predicted to inhibit the innate immune system, we searched for gene ontology (GO) annotations (13, 14) down the tree of high-level terms for virus suppression of host innate immune responses and apoptosis (GO:0039503, GO:0052170, GO:0052309, and GO:0019050). Proteins annotated with these terms, derived from human- and insect-infecting viruses, and with confirmed protein expression reported in UniProt serve as the known innate immune suppressors (Data Set S1). Sequences that lack these gene ontology annotations but that have 20% pairwise alignment identity to

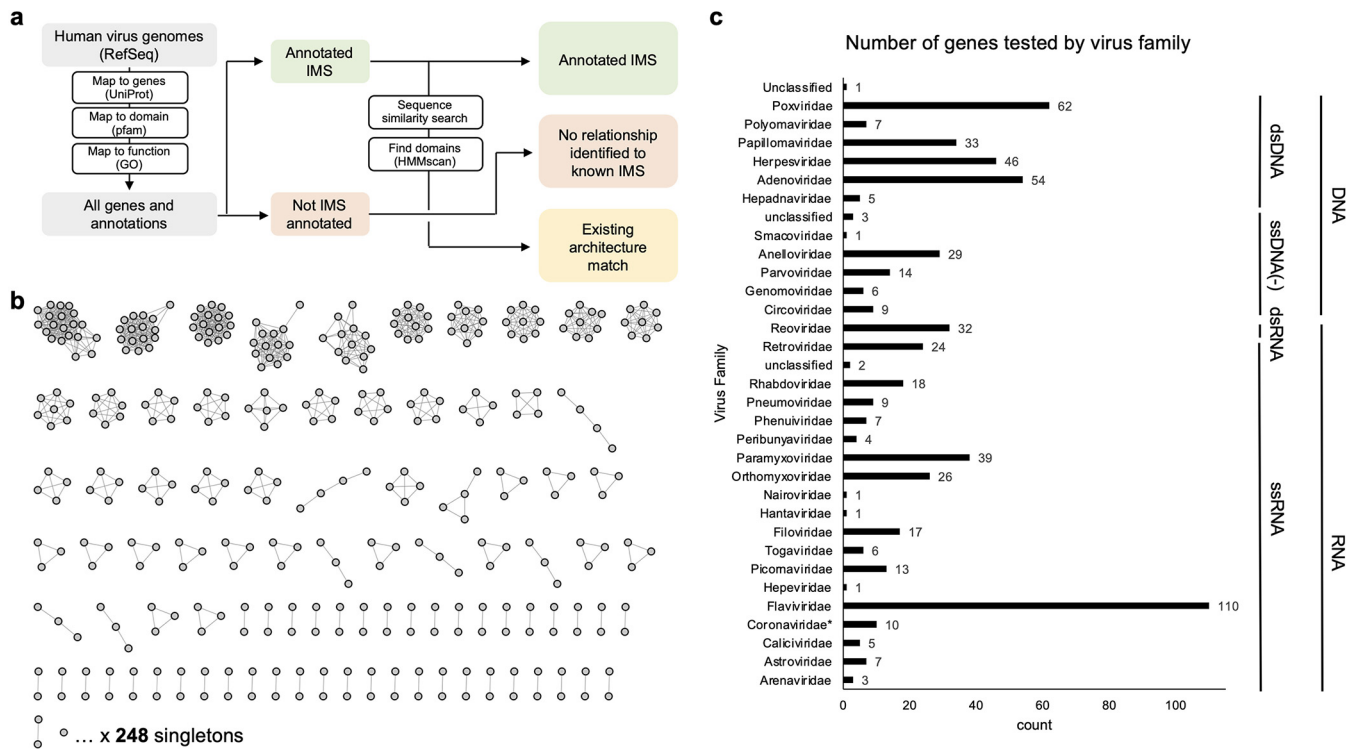


FIG 1 Assembly of a viral gene library to test in immune suppression screens. (a) Overview of the bioinformatic workflow to generate a list of viral proteins for testing. We designated viral genes as (i) immunosuppressive (IMS) by gene ontology (GO) or Pfam search, (ii) predicted IMS based on sequence similarity or permissive hmmscan, or (iii) uncharacterized viral proteins. (b) Sequence similarity network of 605 viral proteins to test clusters of sequence-related proteins and singletons. (c) Distribution of 605 genes by virus family. One hundred ninety-five additional genes from *Coronaviridae* were tested during the COVID-19 pandemic and are not included in this figure.

the known inhibitors form the group of viral proteins with predicted immunosuppressive activities. Functionally related genes with low sequence similarity were identified by deeper models that capture sequence variation across proteins with similar functions (e.g., sharing a family or domain); Pfam is a curated database of hidden Markov models (HMMs) capturing that information (15). We used these HMMs to categorize protein regions as functionally related to known families with high-confidence categorizations that are available on Pfam and UniProt. Lower-confidence domain categorizations can be considered hypothetical and are potential candidates for functional characterization. Overall, we can hypothesize gene functions that are highly distant in sequence similarity from shared domains. Searching our viral protein sequence database (both annotated and unannotated immunosuppressive genes by GO) resulted in 42 proteins as positive hits and 243 predicted inhibitors identified with a more permissive hmmscan.

Overall, our library of 605 genes contains 69 viral immune inhibitors with GO annotations containing immune suppressive (IMS) terms and 89 viral genes with 20% sequence similarity to the IMS genes. Additionally, this library contains 42 known inhibitors determined by containing an immunosuppressive domain by Pfam classification and 201 predicted inhibitors using permissive hmmscan (Data Set S1). Three hundred fifty-eight genes in this library are not predicted to be immunosuppressive. In total, we tested 269 proteins from DNA viruses, 335 proteins from RNA viruses (including retroviruses), and 1 protein from an unclassified hudsavirus (Fig. 1c). The COVID-19 pandemic occurred in the middle of our screening effort described below, which prompted us to test 195 viral genes present in SARS-CoV-2, SARS-CoV, Middle East respiratory virus coronavirus (MERS-CoV), human coronavirus 229E (hCoV-229E), hCoV-NL63, hCoV-OC43, and hCoV-HKU1 (Data Set S1).

High-content screening assay development. To assay the gene library for suppression of human innate immunity, we developed a high-content, medium-throughput assay to reveal the effects of individual viral proteins on the type I interferon

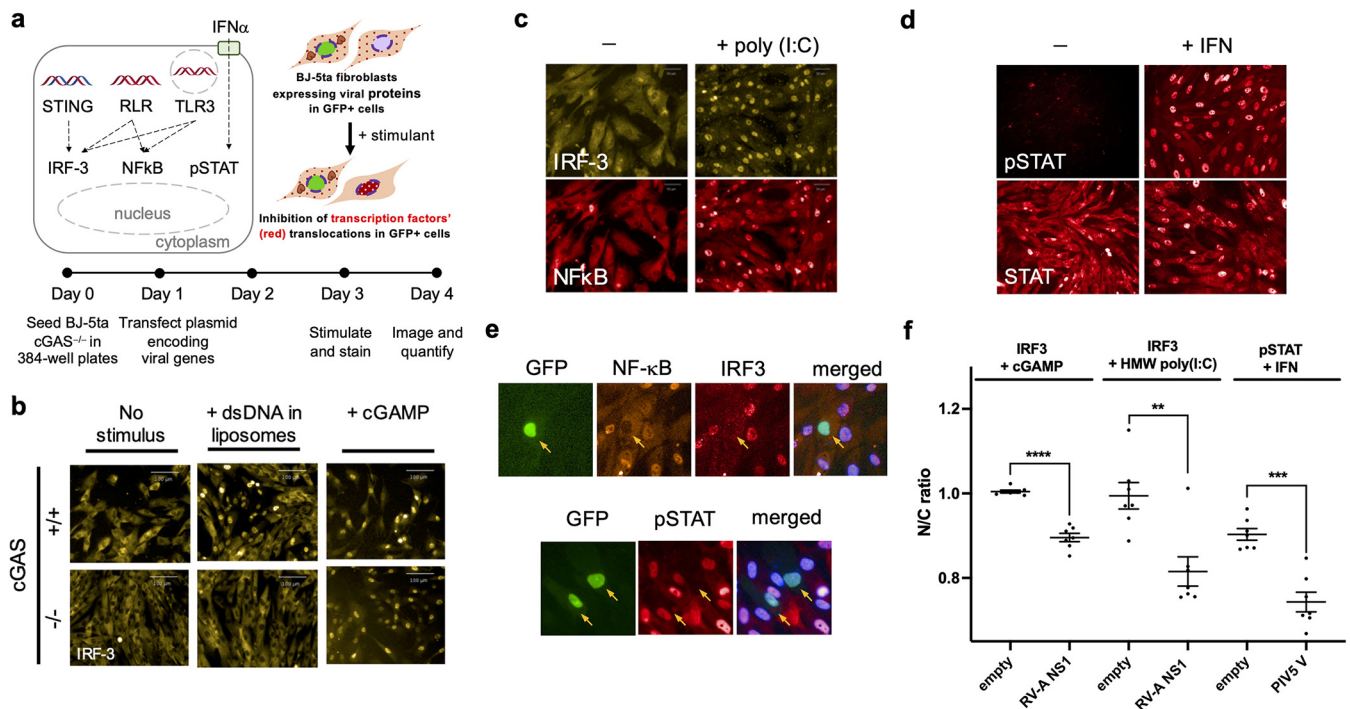


FIG 2 Activation and suppression of antiviral innate immune pathways assayed in fibroblasts via medium-throughput fluorescence microscopy. (a) Innate immune system signaling pathways that respond to viral infection. (Top left) Transcription factors IRF3 and NF- κ B are activated by the presence of nucleic acids in an inappropriate cellular compartment, signifying viral infection. Together, IRF3 and NF- κ B activate expression of IFN- α and IFN- β , which are secreted and locally stimulate the JAK/STAT pathway. IRF3, NF- κ B, and pSTAT1 are all nuclear translocated proteins during signaling. Viruses often encode proteins that disrupt these pathways, by directly or indirectly inhibiting nuclear translocation, or by causing degradation of the transcription factor. (Top right) The pathways can be initiated *in vitro* by addition of cGAMP (a second messenger), extracellular double-strand RNA (dsRNA), or IFN- α . (Bottom) Experimental workflow for testing virus genes for modulation of the IRF3, NF- κ B, and pSTAT1 signaling pathways. BJ-5ta Δ cGAS cells are transiently transfected with a viral gene expression vector, treated with various stimuli, stained with antibodies against IRF3, NF- κ B, and/or pTyr701-STAT1, incubated with secondary antibodies, and then imaged. (b) Knockout of cGAS prevents transfection-mediated stimulation of IRF3 translocation while allowing downstream activation of IRF3 via cGAMP. Double-stranded DNA (dsDNA) in the cytoplasm activates cGAS to create the cyclic dinucleotide cGAMP, which then acts on STING to activate IRF3. Parental cGAS⁺ BJ-5ta cells show nuclear IRF3 translocation in response to transfected DNA and exogenous cGAMP, while BJ-5ta cells with a CRISPR cGAS knockout show an IRF3 response only after treatment with cGAMP. This allowed us to assay elements of the STING/IRF3 pathway without interference by transfected DNA. (c) BJ-5ta Δ cGAS cells treated with poly(I:C) show translocation of IRF3 and NF- κ B into the nucleus. (d) IFN- α treatment caused translocation of cytoplasmic nuclear STAT1 and pSTAT1 into the nucleus. For this study, we chose to stain only for pSTAT1. (e) Images of BJ-5ta Δ cGAS cells that were cotransfected with plasmids encoding GFP and rotavirus A (RV-A) nonstructural protein 1 (NS1) and stained for NF- κ B and IRF3. Cells were also cotransfected with plasmids encoding GFP and parainfluenza virus 5 (PIV5) V protein and stained for pSTAT1. Only transfected cells (arrows) show inhibition of nuclear localization or formation of phospho-STAT1. (f) Quantitative results for nuclear-to-cytoplasmic (N/C) ratio for IRF3 and pSTAT1 for BJ-5ta Δ cGAS cells expressing no viral protein, rotavirus A NS1, or PIV5 V protein. Some cells expressing these proteins were treated with cGAMP, HMW poly(I:C), or IFN- α to activate the immune signaling axes of interest. Viral inhibition of transcription factor translocation resulted in lower N/C ratio in the presence of stimuli. Data are means and standard deviations (SD) for >5 replicates. Statistical significance values were calculated with an unpaired t test. ****, $P < 0.0001$; ***, $P < 0.001$; **, $P < 0.01$.

pathways. The three main signaling cascades tested are the TLR3 (Toll-like receptor 3)-, cyclic GMP-AMP synthetase (cGAS)-2',3' cyclic GMP-AMP (cGAMP)-STING-, and JAK/STAT-mediated pathways. These three signaling axes (Fig. 2a) respond to foreign endosomal RNA, cytosolic DNA, and interferon (IFN), respectively. When the cell senses foreign DNA and RNA via pattern recognition receptors, multiple signaling cascades lead to nuclear translocation of the cytosolic proinflammatory transcription factors NF- κ B, interferon regulatory factor 3 (IRF3), and pSTAT, which produces antiviral responses. We chose these signaling axes because the pathways and numerous viral inhibitors have been well studied in the literature (1, 2). We developed conditions in which the nuclear/cytoplasmic localization of IRF3 and NF- κ B could be simultaneously visualized using non-cross-reacting primary and secondary antibodies (16).

All viral genes were synthesized and placed in a plasmid vector to promote constitutive expression upon transfection. We chose nontransformed, tert-immortalized BJ-5ta fibroblasts as our host cell type, as these cells are amenable to imaging-based screening and high-throughput screens (16). Furthermore, BJ-5ta fibroblasts encode relatively intact innate immune pathways compared to other cell types (e.g., HEK293T

cells express low levels of STING [17] and TLR3 [18]). Since DNA transfection alone stimulates the cGAS-STING pathway (Fig. 2e), we generated a CRISPR knockout of cGAS (BJ-5ta Δ cGAS; see Materials and Methods). In this cell line, DNA transfection-mediated stimulation of IRF3 nuclear transport was essentially undetectable (Fig. 2b).

To assess the effect of a particular gene on innate immune signaling pathways, BJ-5ta Δ cGAS cells (Fig. 2a) were seeded in 384-well plates and cotransfected with a viral gene expression vector and a green fluorescent protein (GFP) expression plasmid. Coexpression of viral proteins and GFP was highly correlative (Fig. S1). Extracellular poly(I-C) or cGAMP was used to stimulate signaling via the TLR3 or STING pathway, respectively. These stimuli caused localization of IRF3 and/or NF- κ B from the cytoplasm to the nucleus (Fig. 2d and e). BJ-5ta Δ cGAS cells were also treated with IFN- α to initiate STAT1 phosphorylation and nuclear translocation (Fig. 2f). Two days after stimulation, cells were stained either with a mixture of NF- κ B and IRF3 or with anti-pSTAT1 (phospho-pSTAT1 Tyr701) antibodies. Based on the timing of the induced response, cells were fixed, stained with antibodies directed against relevant transcription factors, and imaged. Fields of cells were scored by automated image processing for expression of a GFP transfection marker and the nuclear/cytoplasmic distribution of NF- κ B, IRF3, or pSTAT1 (Fig. 2c to e). Hits were identified based on inhibition strengths of cells transfected with a viral protein-encoding vector compared to an empty vector control (see Materials and Methods and the supplemental material). Using this assay, we tested rotaviral A (RV-A) nonstructural protein 1 (NS1), which induces IRF3 degradation (19). Significant inhibitory responses of IRF3 translocation were observed when cells were treated with cGAMP or poly(I-C) (Fig. 2f). We also tested parainfluenza virus (PIV) 5 V protein, a known JAK/STAT pathway inhibitor, and observed strong inhibition of pSTAT translocation when the BJ-5ta Δ cGAS cells were treated with IFN- α (20). Therefore, this workflow is suitable for screening our viral gene library for immunosuppressive functions.

High-content imaging assays identified known and predicted viral inhibitors.

Using the described assays, we tested 605 viral genes from our library (Fig. 1c) and an additional 195 coronaviral genes we obtained during the COVID-19 pandemic. Applying a “stringent” cutoff ($P < 0.05$) by comparison to the no-stimulus control (Fig. S2 to S4) resulted in clear enrichment of 79 viral proteins that inhibited transcription factor translocation (Fig. 3a; Data Set S3). Only a few proteins that strongly inhibited NF- κ B translocation in the cGAMP-stimulated assay were obtained (Fig. 3a; Fig. S2b). Overall, we obtained more IRF3 translocation inhibitors than NF- κ B translocation inhibitors in the STING- and TLR3-mediated pathways, and our assays revealed more pathway-specific inhibitors than proteins that inhibit multiple signaling axes (Fig. 3b).

The list of 79 viral proteins included numerous known inhibitors of innate immunity (Data Set S3). Specifically, 3 proteins were annotated with our selected IMS gene ontology terms, and 16 proteins were related to positive IMS genes by sequence similarity. Seven proteins were identified that contain domains known to inhibit immune function, and 18 viral proteins were inferred from hmmscan searches of known inhibitors. Two viral proteins, flaviviral NS4B and parvoviral VP1, were hits that contain domains with homology to known human proteins. Examples of previously reported inhibitors included cowpox viral poxin, which strongly inhibited IRF3 translocation when the cells were stimulated with cGAMP but not other stimuli (Fig. S5a). This observation is consistent with poxin nuclease's cGAMP-cleaving activity (21). W protein from the henipavirus Nipah virus inhibited nuclear translocation of IRF3 when stimulated with HMW poly(I-C) (Fig. S5b). This protein has been demonstrated to inhibit phosphorylation of IRF3 (22). Other strong hits include several phenuiviral nonstructural proteins (NSs), picornaviral 3C proteases (3C^{pro}), and rhabdoviral matrix proteins (M) (Fig. 3c; Fig. S5). NSs from phenuivirus, specifically, sandfly fever Sicilian virus and heartland virus, are known to block the DNA-binding domain of IRF3 (23, 24). Our assays demonstrated that NSs from sand fever Turkey virus and heartland virus both inhibited IRF3 translocation when stimulated with poly(I-C). Moreover, heartland virus NSs inhibited cGAMP-stimulated IRF3 translocation, while the protein encoded by sand fever Turkey virus

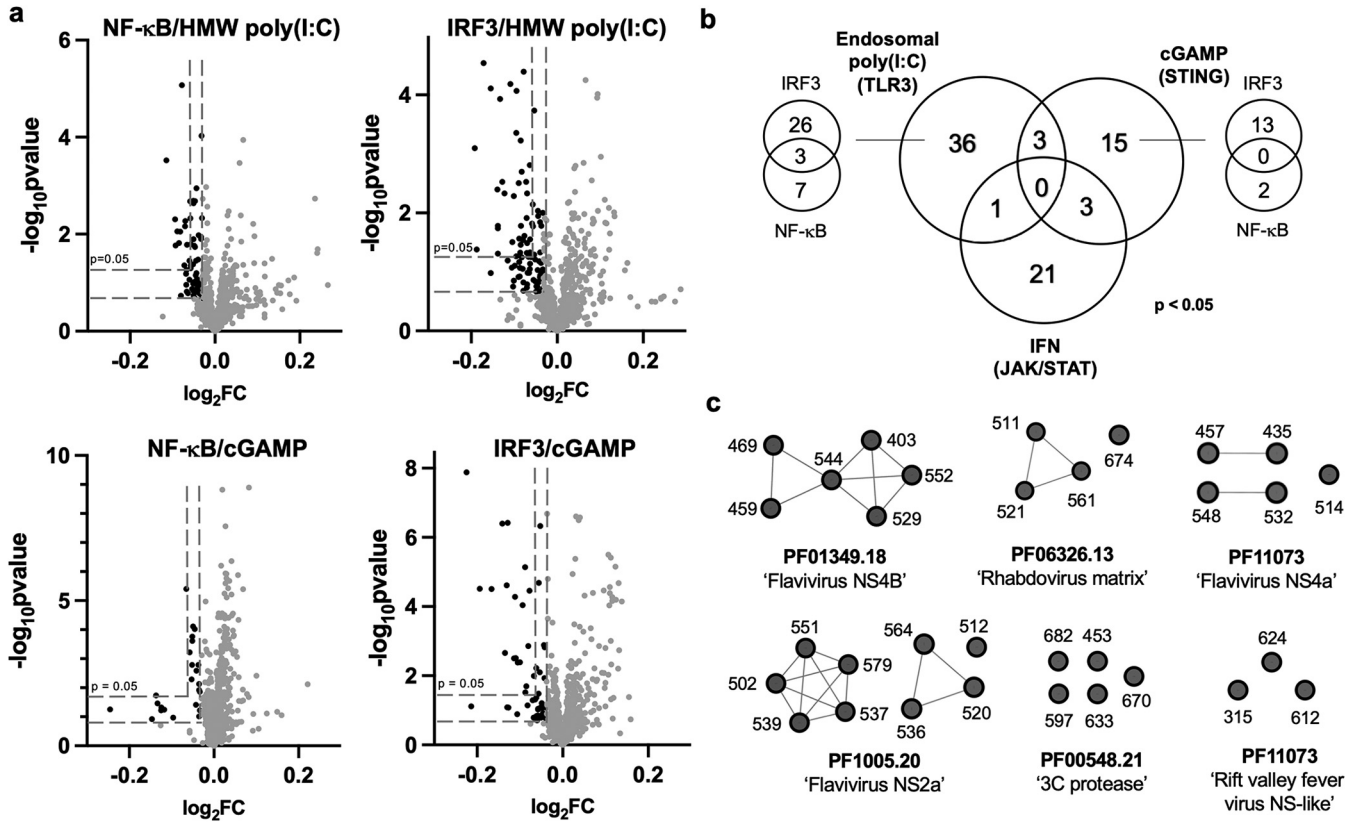


FIG 3 (a) Volcano plots highlight hits with stringent ($P < 0.05$) and permissive ($P < 0.1$) cutoffs. Eight hundred genes (including the 195 coronavirus genes) are plotted. Cutoff values for \log_2 fold change ($\log_2 FC$) and P values were determined by comparing the data to the corresponding no-treatment controls, which do not result in robust nuclear translocation of transcription factors. Results for no treatment controls and IFN- α -treated cells are depicted in Fig. S2 to S4. Raw source data are provided in Data Set S2. (b) Venn diagram depicting 79 stringent hits ($P < 0.05$) among 800 viral genes across the four assays. For the endosomal HMW poly(I:C)- and STING (cGAMP)-stimulated pathways, the additional Venn diagrams report the number of viral genes that inhibited IRF3 and/or NF- κ B. (c) Examples of sequence-related positive innate immune inhibitors, grouped by Pfam domains, found in our screen and/or among inhibitors reported in the literature. The full list of permissive hits can be found in Data Set S3. Plots depicting $\log_2 FC$ and statistical significance for selected hits are compiled in Fig. S5.

inhibited it to a lesser extent. Finally, we identified 14 coronavirus genes as immune inhibitors, including SARS-CoV-2 Orf3a (IRF3, poly(I:C) treated), Nsp10 (pSTAT, IFN- α -treated), and the nuclear transport inhibitor Orf6 (pSTAT, IFN- α treated) (Fig. 3a; Fig. S5; Data Set S3). Overall, our assays recorded several known viral hits, despite differences in cell lines, experimental conditions, and detection methods.

To further reveal trends of viral proteins that inhibit the innate immune pathways, we generated a separate list of 232 immunosuppressive proteins identified with a more permissive cutoff ($P < 0.1$) (Fig. 3a; Fig. S5; Data Set S3). We found large clusters of hits belonging to several flaviviral nonstructural proteins (25), such as 6 NS4B, 9 NS2a, and 5 NS4a sequences (Fig. 3c). Other large clusters of protein hits include the aforementioned proteases and matrix proteins. We observed the same trend that viral proteins tend to be more pathway-specific inhibitors under our conditions (Fig. S6). Notable proteins that broadly inhibited all three signaling pathways include SARS-CoV-2 Orf6, togavirin from Western equine encephalitis virus, and matrix protein from Jurona vesiculovirus. Additional coronaviral genes that inhibited immune pathways to a weaker extent include SARS-CoV Orf6 (26) and SARS-CoV-2 protease Nsp5.

Mechanistic investigations into known, predicted, and new viral inhibitors.

Protease activity is required for innate immune suppression by newly identified candidate proteases. 3C^{pro} from the picornaviral family are known to cleave various host factors in innate signaling pathways (27). For example, hepatovirus A (HAV) 3C^{pro} cleaves a bridging adaptor protein involved in IFN antiviral response in HEK293T cells (28). In cGAMP-stimulated BJ-5ta Δ cGAS cells, we observed strong inhibition of IRF3 translocation when 3C^{pro}

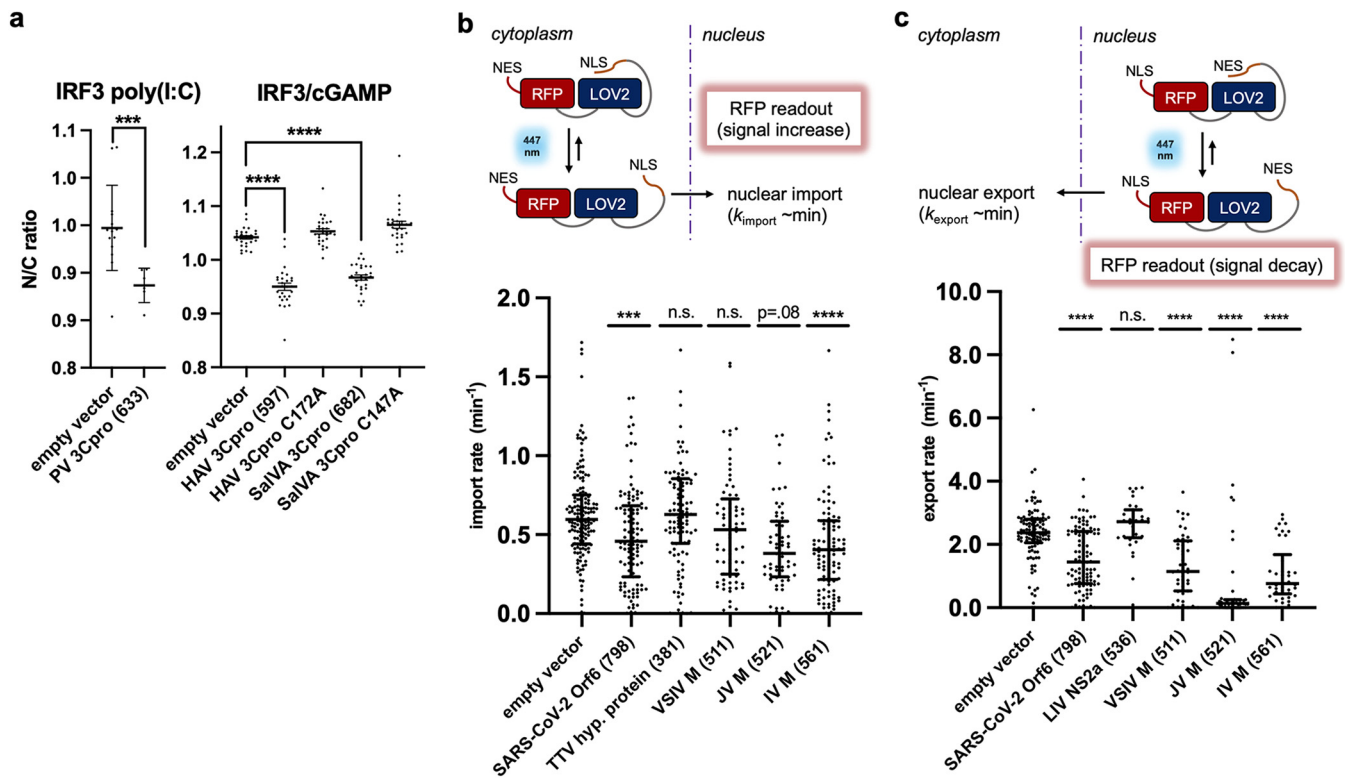


FIG 4 (a) Consolidated imaging results for nuclear translocation of IRF3 in cGAMP-stimulated BJ-5ta Δ cGAS cells transfected with wild-type and variant viral genes. Cells expressing parechovirus (PV) 3C^{pro} exhibited lowered nuclear IRF3 intensity when stimulated with poly(I:C). Cells transfected with hepatitis A (HAV) 3C^{pro} and salivirus A (SalVA) 3C^{pro} exhibited lower nuclear IRF3 intensity, while their corresponding active site mutants did not exhibit these effects. (b and c) Matrix proteins from viruses in the family *Rhabdoviridae* inhibit nuclear import and export of RFP probe in U2OS cells. In the presence of 447-nm light, a fusion protein with a LOV2 domain undergoes a conformational change that reveals either a nuclear localization signal (NLS) (b) or nuclear export signal (NES) (c) that increases or decreases nuclear RFP localization. Import and export rates were measured in single cells with a confocal microscope. These results demonstrated that M from vesicular stomatitis virus (VSV), Isfahan virus (IV), and Jurona vesiculovirus (JV), which scored positive in our assay, inhibited nuclear import and export of proteins as expected. Torque teno virus 10 (TTV) hypothetical protein (381) and louping ill virus (LIV) NS2a (536) were also tested in the assay as additional negative controls. Data are means and SD for >5 replicates or cells. Statistical significance values were calculated with an unpaired *t* test. ****, $P < 0.0001$; ***, $P < 0.001$.

from parechovirus, hepatitis A, and salivirus A were expressed (Fig. 4a). 3C proteases from parechovirus and salivirus A have not been characterized to our knowledge. To demonstrate that the observed fold change is due to the proposed protease activity of viral proteins, we repeated our assay with the two candidate proteases and their corresponding catalytic cysteine variants (Fig. 4a). These mutants lost the inhibitory phenotype in our assay. Our results indicate that these other viral proteases, although weakly similar by sequence, are also capable of suppressing innate immune pathways.

Newly identified matrix proteins (M proteins) inhibit nuclear transport. M proteins encoded by the rhabdovirus family were among our top hits. M from vesicular stomatitis virus (VSV) blocks host gene expression by binding to nuclear transport factors RAE1 and Nup98 and inhibits poly(A) mRNA export (29). We find that M from Isfahan virus [IRF3 and NF- κ B, poly(I:C) treated], Jurona vesiculovirus (IRF3, cGAMP treated), and vesicular stomatitis Indiana virus [NF- κ B, poly(I:C) treated] inhibited translocation in our imaging-based assays. Based on this result, we hypothesized that M from Isfahan and Jurona vesiculovirus also block nuclear import and export. We tested these matrix proteins in an optogenetics-based assay (30–32) that measures the rate of import and export of a fluorescent protein probe (Fig. 4b and c). In this assay, U2OS cells stably express a photoactivatable nuclear transport signal fused to a red fluorescent protein with a constitutive nuclear export or import signal. For example, we measure a viral protein's effect on nuclear import rate by expressing our viral proteins in U2OS cells that stably express a photoactivatable nuclear import sequence fused to a cytoplasmic red fluorescent protein (RFP) (Fig. 4b). We found that the SARS-CoV-2 Orf6 (33), VSV M

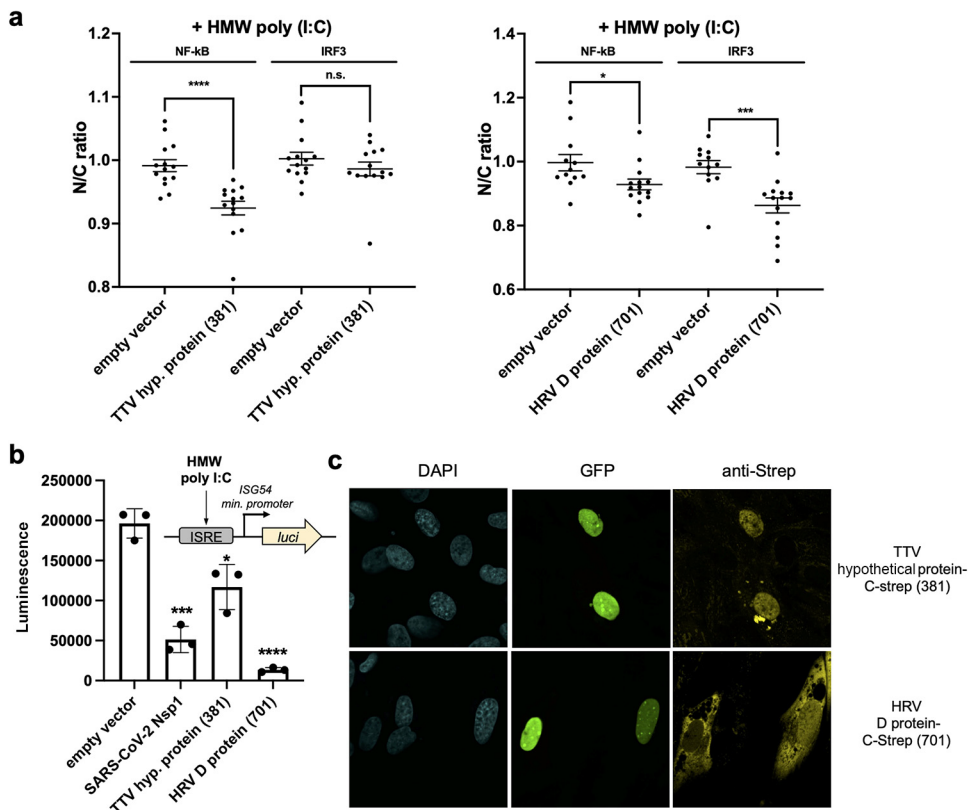


FIG 5 (a) High-content imaging results for nuclear translocation of IRF3 when BJ-5ta Δ cGAS cells express TTV hypothetical (hyp.) protein or HRV3 D protein. Cells transfected with these genes exhibited lower nuclear IRF3 intensity. Data are means and SD for >5 replicates. Statistical significance values were calculated with an unpaired *t* test. ****, $P < 0.0001$; ***, $P < 0.001$; *, $P < 0.05$. (b) Reduced luminescence readout was observed for the TTV hypothetical protein and HRV D protein in A549-Dual (InvivoGen) cells when HMW poly(I:C) was used to stimulate the cells. ISRE, interferon stimulated response element; *lucif*, gene encoding luciferase. Data are means and SD for 3 replicates. Statistical significance values were calculated with an unpaired *t* test. ****, $P < 0.0001$; ***, $P < 0.001$; *, $P < 0.05$. (c) Cellular localization of the hypothetical TTV and HRV D proteins seen by immunofluorescence staining of C-terminally streptavidin-tagged proteins of interest expressed in BJ-5ta Δ cGAS cells. Results of SDS-PAGE of the overexpressed and purified viral proteins are shown in Fig. S7.

protein, and the uncharacterized rhabdoviral M proteins impaired bidirectional transport, consistent with blocking nuclear pores via interactions with Nup98.

We also identified several viral genes to which no immune inhibitory effects have been attributed to the best of our knowledge. We found 38 and 115 such genes under stringent and permissive cutoffs, respectively (Data Set 3). Many of these proteins have alternative functions in an infection, such as nucleoproteins, glycoproteins, capsid proteins, and matrix proteins. For example, we identified capsid proteins (Pfam accession no. [PF02956](#)) from four different strains of torque teno virus that inhibited the STING and JAK/STAT pathways (Data Set S3). Two paramyxoviral glycoproteins (Pfam accession no. [PF00523](#)) encoded by Hendra virus and human respirovirus 3 inhibited the TLR3 pathway.

Two proteins with no previously known function are a hypothetical protein with an intrinsically disordered domain encoded in torque teno virus 10 (TTV10) (NCBI accession no. [YP_003587850](#)) and an intrinsically disordered protein from human respirovirus 3 (HRV3) (NCBI accession no. [NP_599250](#)) (Fig. 5a). TTV is reported to be a prevalent virus present in most humans, yet it is understudied along with other human anelloviruses due to difficult cultivating conditions (34). We tested these proteins in A549-Dual reporter cells (InvivoGen), which report IRF translocation via a luciferase readout (Fig. 5b). We observed that expression of TTV hypothetical protein and HRV disordered protein inhibited interferon-stimulated response element (ISRE)-driven gene expression when

the cells were stimulated with poly(I-C). We next immunostained the streptavidin (Strep)-tagged versions of the two proteins overexpressed in BJ-5ta Δ cGAS cells and observed that TTV hypothetical protein is associated with the nuclear compartment (Fig. 5c; Fig. S7). However, this protein does not affect nuclear transport (Fig. 4b) in our optogenetics assay. These data confirm the ability of our screen to identify traits of previously uncharacterized viral proteins.

DISCUSSION

In this work, we characterized the ability of 800 viral proteins encoded by a diverse set of viruses to suppress host intracellular innate immune signaling pathways using a high-content, medium-throughput cell-based assay. We examined the nuclear localization of the transcription factors IRF3, NF- κ B, and pSTAT1, which play key roles in the elaboration of the type I interferon response to viral infection and which are major targets for inhibition by other viruses (35). To evaluate our assays, we undertook a bioinformatic approach that broadly searched databases of human-, mammal-, and insect-infecting viruses in order to maximize the diversity of viruses we test. Our library was designed to contain known immune inhibitors as well as proteins that are related by sequence similarity or by containing homologous Pfam domains. We also included viral proteins with no predicted immunosuppressive function. Immune inhibitors within this class could be viral proteins that have an alternative function (e.g., capsid proteins) or in which no function has been assigned at all (e.g., hypothetical proteins). Altogether, this library allows us to benchmark the strengths and weaknesses of our assay, as well as provide an avenue for discovering new viral immune inhibitors. We note that this library will be available for other medium- and high-throughput assays, such as transcription-based reporter assays.

We developed an image-based screen to quantify the effects of viral proteins on nuclear translocation of various proinflammatory transcription factors. Viruses act on these pathways by a variety of mechanisms, such as specific inhibition of upstream signal transduction proteins, general inhibition of nuclear import, and enhancement of host factor degradation. Our assays involved transfection of a nontransformed cell line with expression vectors carrying each gene, followed by addition of a stimulator of innate immune signaling, and then immunofluorescence staining and automated image processing. This workflow allows rapid testing of diverse viral genes and bypasses viral culturing. As such, it allows us to test viral genes from any virus under low-containment conditions. Individual key signaling pathways were tested depending on the stimuli, and these assays allow us to probe effects of viral proteins on different stages of innate immune response. Some proteins may require concurrent viral infection for function and proper levels and thus appear as false negatives. However, our single-protein assays concur with practices standard in the field (36, 37) and allow a larger-scale analysis, as carried out here. We anticipate that these results will help steer further experimentation on the corresponding virus if possible.

Our assay reproduced numerous hits previously reported in the literature, such as poxin protein, rotavirus NS1, and numerous flaviviral protein clusters such as NS4B and NS2a, thereby confirming its value. While many hits were specific to one signaling axis, such as poxin and flaviviral NS2a, we did observe several hits that broadly blocked protein translocation, such as proteins that block nuclear transport. We focused on proteases from the 3C family and M proteins from rhabdoviruses, as they were consistent hits, and we investigated their mechanisms via mutagenesis and nuclear import/export assays. These experiments confirmed that predicted viral inhibitors identified from our assay exhibited the same immunosuppressive activities as previously characterized homologues. Furthermore, these results suggested our assay could facilitate mechanistic investigations and could also be optimized for assays to test for small molecule inhibitors of viral innate immune suppression.

Our screen also identified several hits that have not yet been assigned as immune inhibitors. Among these hits are capsid proteins from torque teno viruses and several

paramyxoviruses. We also found paramyxoviral glycoproteins to be highly represented in our hit results. Viral proteins are known to be multifunctional, including structural proteins such as matrix or nucleocapsid proteins that may play a role in regulating innate immune responses (38, 39). We also identified hypothetical and uncharacterized proteins for which no functions have been elucidated to the best of our knowledge, such as the hypothetical protein encoded by torque teno virus 10. The results presented in our screen could guide future work to further dissect their mechanisms, potentially in the context of an infection. Our discovery of potential inhibitors from torque teno virus highlights the importance of culture-independent assays for functional characterization of proteins. Anelloviruses establish persistent infections in most healthy humans, and efforts to establish a reliable culture condition and to engineer these viruses for delivering payload are actively being pursued (40). Assays similar to the ones presented in this study could forward our understanding and engineering of this viral family for translational applications.

Innate immune suppression may correlate with asymptomatic spread in addition to pathogenicity (41). By carrying out these experiments, we sought to provide tools for rapid, functional characterization of viral proteins in the era of metagenomics. This will further our capacity to link new viral sequences and function. Coupled with infection studies and/or independent secondary assays, our study could enable rapid testing of viral genes in assays for innate immune suppression, making early-stage evaluation of emerging and understudied viruses possible.

MATERIALS AND METHODS

Culturing the BJ-5ta human fibroblast cell line. BJ-5ta cells were purchased from ATCC (CRL-4001) and cultured in the manufacturer-recommended medium of 4:1 Dulbecco's modified Eagle medium (DMEM)-M199 with 10% fetal bovine serum (FBS) (72% DMEM [ATCC 30-2002], 18% M199 [Thermo Fisher Scientific 11150059], 10% U.S. origin FBS [GenClone no. 25-514] and 10 $\mu\text{g}/\text{mL}$ hygromycin B [InvivoGen ant-hg-1]). Cells were cultured in T-25, T-75, and T-150 cell culture-treated flasks with vented caps (Corning) at 37°C and 5% CO_2 . Cells were passaged every 3 to 4 days at 70 to 90% confluence to 30% confluence.

Seeding BJ-5ta cells into 384-well plates. BJ-5ta ΔcGAS cells were lifted from T-150 culture flasks using 0.25% trypsin (VWR 45000-664) for 5 to 10 min; then, the trypsin was quenched with 2 \times volume of culture medium and transferred to 50-mL Falcon tubes. The cell suspension was centrifuged in a swinging-bucket rotor at 300 $\times g$ for 6 min at room temperature. The supernatant was discarded by aspiration and cells were resuspended in a small amount of culture volume and counted with a Bio-Rad TC20 automated cell counter. Cells were diluted to 60,000/mL, and 40 μL of diluted cell suspension was added from a reservoir to all wells except the outer row (i.e., rows B to O in columns 2 to 23 were used) of tissue-culture-treated black CellCarrier-384 Ultra microplates (Perkin Elmer 6057302) using a 12-channel electronic multichannel 200- μL pipettor (Sartorius). Plates were then centrifuged at 200 $\times g$ for 4 min at room temperature and incubated overnight. Typically, about 2,000 to 5,000 cells per well were seeded, and about 200 to 800 were transfected, as determined by expression of GFP.

Cotransfection of virus gene plasmids and GFP into BJ-5ta cells. Thirty to 60 min prior to transfection, BJ-5ta culture medium (4:1 DMEM-M199 with 10% FBS) was replaced with an equal volume of prewarmed antibiotic-free transfection medium (4:1 DMEM-M199 with 20% FBS; 64% DMEM, 16% M199, 20% FBS). Transfection mixes were prepared according to manufacturer protocol (Lipofectamine 3000; Thermo Fisher no. L3000015) with final concentrations of 1 μg DNA and 4 μL GeneXPlus in 100 μL of Opti-MEM I reduced-serum medium. Briefly, GeneXPlus (ATCC ACS-4004), plasmid DNA (200 ng/ μL), and Opti-MEM I reduced-serum medium (Thermo Fisher no. 31985062) were warmed to room temperature and vortexed gently. Plasmid DNA was aliquoted into sterile microcentrifuge tubes at a 3:1 ratio of virus gene plasmid to GFP-containing plasmid. Opti-MEM was quickly mixed with GeneXPlus, and the appropriate volume was added to each DNA aliquot and mixed briefly by gentle pipetting. GeneXPlus-DNA complexes were formed at room temperature for 15 to 20 min. Transfection mixtures were then added to each well at 10% final volume (4.4 μL transfection mixture was added to 40 μL transfection medium). Plates were centrifuged at a relative centrifugal force (RCF) of 200 for 4 min at room temperature to collect all the transfection mixture into the medium, and the medium was briefly mixed by tilting the plate back and forth. Cells were incubated with transfection mixture at 37°C and 5% CO_2 for 24 h to allow DNA to enter cells. Transfection medium was then exchanged for fresh culture medium, and cells were further incubated for another 24 h prior to stimulation with innate immune stimuli and fixation as described above.

Homozygous knockout of cGAS in BJ-5ta cells. CRISPR was used to introduce a frameshift mutation at position 13 of exon 1 of cyclic GMP-AMP synthetase (cGAS) in BJ-5ta cells. Three different Synthego-designed guide RNAs were each cotransfected with Cas9-containing plasmid (Synthego) into BJ-5ta cells (ATCC CRL-4001) using Lipofectamine 3000. After 48 h, samples were removed from each knockout pool for inference of CRISPR edits (ICE) analysis to assess gRNA efficiency, which was 1 to 6%.

The knockout pool with 6% gRNA efficiency (gRNA 2) was diluted to a density of 0.5 cells/100 μ L and plated into 96-well plates for clonal expansion. Colonies grown from a single cell were visually identifiable after 3 weeks. After 8 weeks, the cGAS locus was sequenced in each clonal colony to identify colonies with homozygous indels. One homozygous knockout colony was identified from 20 screened colonies. Homozygous knockout in successful colonies was confirmed via Western blotting for cGAS protein.

Stimulation of innate immune signaling. The BJ-5ta Δ cGAS cell line was used for innate immune signaling experiments. This cell line demonstrated a strongly reduced level of background innate immune signaling that otherwise resulted from introduction of transfecting DNA. In addition, cell transfection efficiency was improved relative to the parental BJ-5ta cells. Cells intended for stimulation with HMW poly(I:C) or LMW liposome-encapsulated poly(I:C) were primed 48 h in advance of stimulation by treating with interferon α 1 (Cell Signaling no. 8927) or interferon α 2b (PBL Assay Science no. 11100-1) at 50 ng/mL (final concentration in the well, 5 ng/mL). Twenty-four hours after treatment with interferon, the cell medium was exchanged to remove external interferon from the cell environment. Different innate immune stimuli were applied to cell medium at 10% culture volume as follows: HMW poly(I:C) (InvivoGen no. tlr-pic) at a concentration of 1 mg/mL for 2 h (final concentration in the well, 100 μ g/mL) was used to stimulate TLR-3 activity by incubation at 37°C and 5% CO₂ for 2 h. cGAMP (InvivoGen no. tlr-nacga23-5) at a concentration of 1 mg/mL (final concentration in the well, 100 μ g/mL) was used to stimulate STING pathway activity by incubation at 37°C and 5% CO₂ for 2 h. Interferon α 1 (Cell Signaling no. 8927) or α 2b (PBL Assay Science no. 11100-1) at a concentration of 50 ng/mL (final concentration in the well, 5 ng/mL) was used to stimulate IFNAR activity by incubation at 37°C and 5% CO₂ for 45 to 50 min. Cell signaling was stopped by fixation as described below.

Cell fixation and immunofluorescent staining. Cells were fixed with 15 μ L of 16% methanol-free formaldehyde (Thermo Fisher no. 28908) added directly to the 45 μ L of cell medium in the wells for a final fixation solution of 4% formaldehyde. After 20 to 25 min incubation, the 4% formaldehyde solution was aspirated and the cells were washed three times with 60 μ L phosphate-buffered saline (PBS) using an automated plate washer (BioTek EL406). Cells to be stained for phospho-STAT1 were further permeabilized with ice-cold 100% methanol (Sigma Aldrich no. 34860), incubated at -20° C for 10 to 15 min, and then washed three times with 60 μ L PBS using an automated plate washer. All primary and secondary antibodies were diluted 1:400 in PBS containing either 2.25% bovine serum albumin (Millipore Sigma no. A2058) or 5% normal goat serum (Abcam no. ab7481) for blocking and 0.15% Triton X-100 (Sigma Aldrich no. T8787) for permeabilization. Fixed cells were stained with 40 μ L diluted primary antibody solution overnight at 4°C. Cells were then washed four times with 60 μ L PBS using an automated plate washer and stained with 40 μ L diluted secondary antibody solution with DAPI (4',6-diamidino-2-phenylindole; Thermo Fisher no. D1306) added to a final concentration of 0.2 μ g/mL. Cells were finally washed four times with 60 μ L PBS using an automated plate washer and sealed using impermeable black plate seals. If not imaged immediately, fixed and stained cells were stored at 4°C for a maximum of 7 days.

Cells treated with interferon α were stained either for phospho-STAT1 (Cell Signaling Technology no. 9167) or for STAT1 (Cell Signaling Technology no. 14994). Cells treated with cGAMP or HMW poly(I:C) were stained simultaneously for IRF3 (Cell Signaling Technology no. 11904) and NF- κ B (Santa Cruz Biotechnology no. sc-8008). IRF3, pSTAT1, and STAT1 primary antibodies were detected using an Alexa Fluor 647-conjugated goat anti-rabbit IgG antibody (Thermo Fisher no. A21245). NF- κ B primary antibody was detected using an Alexa Fluor 568-conjugated donkey anti-mouse IgG secondary antibody (Thermo Fisher no. A10037).

High-content imaging and image segmentation. Fluorescently stained plates were imaged on a PerkinElmer Operetta CLS high-content imaging system with a 20 \times , numerical aperture 0.75 objective. Twenty to 25 sites were imaged in each well, covering 90 to 100% of the well. Each well was imaged for DAPI, GFP, and Alexa 647. Wells treated with cGAMP or poly(I:C) were also imaged for Alexa Fluor 568. Image segmentation was performed using Columbus software (PerkinElmer). Nuclear areas were identified with Columbus method C based on the DAPI channel, and cytoplasmic areas were assigned with Columbus method D based on the Alexa Fluor 647 channel. Average intensities in the GFP, Alexa Fluor 647, and Alexa Fluor 568 (if applicable) channels were calculated for the cytosolic and nuclear areas of each computationally identified cell. Single-cell results were exported from Columbus in CSV format and can be requested from the authors.

Data processing. Briefly, nuclear objects identified by Columbus that correspond to cell debris and artifacts were eliminated based on nuclear morphology. For each transcription factor in a single cell, nuclear localization (nucleus intensity/cytosol intensity) and total cell intensity (nucleus intensity + cytosol intensity) were calculated. Within each well, cells were sorted into GFP-positive or GFP-negative (as a proxy for expression of virus protein) based on average nucleus GFP intensity. The GFP-positive or -negative cutoff was set at twice the median nuclear GFP intensity (the median being within the distribution of the more numerous GFP-negative cells). Within each well, the average nuclear localization or total cell intensity was calculated for the GFP⁺ or GFP⁻ subsets of cells. Subsequently, for each well, the average nuclear localization or total cell intensity for the GFP⁺ cells was normalized to the corresponding average for GFP⁻ cells to obtain a single normalized mean nuclear localization or mean total cell intensity.

Quality control was performed on a plate-by-plate basis as follows. If the mean of either of the two sets of controls containing no virus gene was outside the 20th to 80th percentiles of the plate data as a whole, the data for the aberrant control were discarded. If both no-gene controls were nonaberrant, the two sets of no-gene control data were combined for the following primary fold change calculation and normalization purposes. Additionally, for each individual set of 7 technical replicates, if any data point was more than 3 times the interquartile range higher than the 75th percentile or lower than the 25th percentile, it was removed from the analysis.

Within each plate, the mean and standard deviation of the 7 technical replicates of each virus gene-innate immune stimulus (one type of innate immune stimulus or mock stimulus per plate) combination were calculated. The fold change and corresponding statistical significance of each set of 7 wells for a given virus gene compared to the corresponding empty vector control were calculated. The raw values for the plots in Fig. 3 and Fig. S2 to S4 are presented in Data Set S2 in the columns logfold_T and $-\log_{10}pval$ (see the legend to Data Set S2).

Blind testing and analysis. For each protein, at least three different samples of the corresponding prepared DNA were given to a third party, who randomized and blinded them. The samples were then tested and analyzed, and the identity of each protein was assigned based on comparison to unblind samples run concomitantly.

Nuclear import and export assays. U2OS cell lines (engineered from HTB-96; ATCC) stably coexpressing Halo-H2A and NES-mCherry-LINuS or NLS-mCherry-LEXY were maintained in DMEM (no. 10567022; Thermo Fisher) supplemented with 10% FBS (Thermo Fisher no. A31605 or GenClone no. 25-514) at 37°C in a humidified atmosphere with 5% CO₂. Cells were seeded at 10,000 to 15,000 cells per well in an 8-well chambered coverslip (no. 80826; ibidi) and grown in complete medium for 1 day before cotransfection of the mammalian expression vectors encoding GFP and the viral protein of interest using TransIT-2020 transfection reagent (no. MIR5404; Mirus). After 24 h, the growth medium was replaced with imaging medium: low-glucose (1 g/L) DMEM without phenol red (no. 11054020; Thermo Fisher), supplemented with 10% FBS, 50 IU mL⁻¹ penicillin, 50 μg mL⁻¹ streptomycin, and GlutaMAX (no. 35050061; Thermo Fisher). For nuclear staining, 500 nM JF646-HaloTag ligand (a gift from Luke Lavis) was added to the imaging medium. Image acquisition and kinetics measurements were performed as described previously (32).

Transcriptional reporter assay from A549-Dual cells. A549-Dual (InvivoGen) cells were maintained in F-12K medium (ATCC 30-2004) supplemented with 10% heat-inactivated FBS (Thermo Fisher Scientific no. 10082147), 10 μg/mL of blasticidin, and 100 μg/mL of Zeocin at 37°C in a humidified atmosphere with 5% CO₂. Cells were seeded into 96-well flat-bottom tissue culture-treated culture plates (VWR 10062-900) at a density of 15,000 cells per well in F-12K medium with 10% FBS for 24 h. The next day, plasmids containing viral genes of interest, or empty vector control, were transfected using GeneXPlus according to the manufacturer's protocol. The transfected cells were allowed to grow and express the desired proteins for 48 h before HMW poly(I-C) was added to the cells at a final concentration of 6 μg/mL. The cells were stimulated for 24 h at 37°C in a humidified atmosphere with 5% CO₂. To measure IRF induction, 20 μL of the cell media supernatant was added to 50 μL of QUANTI-Luc assay solution (InvivoGen no. rep-qlc1) in a white 96-well microplate (Greiner no. 655074), and luminescence was immediately measured using a BioTek UV-visible-spectrum (Vis) spectrophotometer.

Immunostaining and purification of overexpressed viral proteins. For immunostaining, BJ-5ta ΔcGAS cells were seeded in 24-well glass-bottom culture plates (Cellvis P24-1.5H-N) at a density of 30,000 cells/well and allowed to grow at 37°C in a humidified atmosphere with 5% CO₂ for 24 h. The next day, plasmids encoding torque teno virus hypothetical protein or human respirovirus 3 D protein were transfected into the cells using GeneXPlus according to the manufacturer's protocol. The transfected cells were allowed to grow for another 48 h. The cells were fixed with 16% methanol-free formaldehyde (Thermo Fisher no. 28908) added directly to the cell medium in the wells for a final fixation solution of 4% formaldehyde. After 20 to 25 min incubation, the 4% formaldehyde solution was aspirated, and the cells were washed three times with 100 μL of PBS manually. Cells were stained for the streptavidin peptide using anti-Strep-tag II antibody (Abcam no. ab76949) diluted 1:2,000 in PBS supplemented with 5% goat normal serum and 1% Triton-X. After incubating overnight at 4°C, the cells were washed three times with 100 μL of PBS manually and stained with diluted secondary antibody solution (Alexa Fluor 568-conjugated goat anti-rabbit IgG antibody) with DAPI (Thermo Fisher no. A-11011). After incubation for 1 h at room temperature, cells were finally washed four times with 100 μL PBS manually and imaged.

For testing protein expression, 1×10^6 HEK293T cells were seeded in 150-mm cell culture dishes and allowed to grow at 37°C in a humidified atmosphere with 5% CO₂ for 24 h. The next day, plasmids encoding empty vector, torque teno virus hypothetical protein, or human respirovirus 3 D protein were transfected into the cells using TransIT-LT1 (Mirus Bio) according to the manufacturer's protocol. After 48 h, the cells were lifted with a cell lifter and washed with ice-cold PBS, and the pellet was frozen at -80°C at least 15 min before protein purification. To purify the proteins, the frozen cell pellet was allowed to thaw on ice for 30 min. Ten milliliters of lysis buffer (IBA LifeSciences buffer W supplemented with 0.5% NP-40 substitute and one tablet of protease inhibitor [cComplete EDTA-free protease inhibitor cocktail; Sigma Millipore]) was added to the thawed pellet. The mixture was passed through a syringe needle ~ 30 times before centrifugation at 12,000 rpm at 4°C. The supernatant was passed through a column packed with Strep-Tactin resin (IBA LifeSciences no. 2-1208-010) and washed with IBA LifeSciences buffer W (NC0612462; three times with 10 mL each). The bound proteins were eluted from the column with 10 mL of IBA LifeSciences elution buffer and concentrated with a centrifugal concentrator. The concentrated soluble fraction was analyzed by SDS-PAGE or Western blotting using standard methods.

Data availability. All data and resources are available from the corresponding authors upon reasonable request.

SUPPLEMENTAL MATERIAL

Supplemental material is available online only.

DATA SET S1, XLSX file, 0.1 MB.

DATA SET S2, XLSX file, 0.7 MB.

DATA SET S3, XLSX file, 0.1 MB.

FIG S1, PDF file, 0.5 MB.

FIG S2, PDF file, 0.3 MB.

FIG S3, PDF file, 0.3 MB.

FIG S4, PDF file, 0.2 MB.

FIG S5, PDF file, 0.4 MB.

FIG S6, PDF file, 0.03 MB.

FIG S7, PDF file, 1 MB.

ACKNOWLEDGMENTS

This research was sponsored by the Office of the Director of National Intelligence (ODNI), Intelligence Advanced Research Projects Activity (IARPA) Functional Genomic Characterization of Threats (Fun GCAT) program through the Army Research Office (ARO) and under grant number W911NF-17-2-0092. The views and conclusions contained in this document are those of the authors and should not be interpreted as representing the official policies, either expressed or implied, of ODNI, IARPA, ARO, or the U.S. Government. Tai L. Ng is an Open Philanthropy Awardee of the Life Sciences Research Foundation. Tae Yeon Yoo is supported by NIH/NIGMS postdoctoral fellowship F32GM131585.

We thank Devin Burrill for editing the manuscript.

T.L.N., E.J.O., H.S.W., and T.M. performed plasmid purification, screens, data collection, and analysis. T.L.N. and T.Y.Y. performed optogenetic assays, and T.Y.Y. analyzed the results. Y.K. constructed the BJ-5ta cGAS knockout strain and expression vector design. E.J.O., P.D.K., P.M., T.J.M., T.Z.C., and J.Z. contributed to the screening methodology. N.J.R., R.L.C., and D.S.M. performed bioinformatics analysis. T.B. and C.M. contributed to image processing. T.L.N., E.J.O., and N.J.R. wrote the manuscript. J.C.W. was primarily responsible for initial project conceptualization and subsequent direction with assistance from P.A.S., T.J.M., D.S.M., and J.I.G. P.A.S. was responsible for the overall project administration.

We declare that we have no conflicts of interest.

REFERENCES

- Crowl JT, Gray EE, Pestal K, Volkman HE, Stetson DB. 2017. Intracellular nucleic acid detection in autoimmunity. *Annu Rev Immunol* 35:313–336. <https://doi.org/10.1146/annurev-immunol-051116-052331>.
- Lee H-C, Chaturanga K, Lee J-S. 2019. Intracellular sensing of viral genomes and viral evasion. *Exp Mol Med* 51:1–13. <https://doi.org/10.1038/s12276-019-0299-y>.
- Nelemans T, Kikkert M. 2019. Viral innate immune evasion and the pathogenesis of emerging RNA virus infections. *Viruses* 11:961. <https://doi.org/10.3390/v11100961>.
- Katze MG, He Y, Gale M. 2002. Viruses and interferon: a fight for supremacy. *Nat Rev Immunol* 2:675–687. <https://doi.org/10.1038/nri888>.
- Versteeg GA, García-Sastre A. 2010. Viral tricks to grid-lock the type I interferon system. *Curr Opin Microbiol* 13:508–516. <https://doi.org/10.1016/j.mib.2010.05.009>.
- Domingo-Gil E, Toribio R, Nájera JL, Esteban M, Ventoso I. 2011. Diversity in viral anti-PKR mechanisms: a remarkable case of evolutionary convergence. *PLoS One* 6:e16711. <https://doi.org/10.1371/journal.pone.0016711>.
- Gréninger AL. 2018. A decade of RNA virus metagenomics is (not) enough. *Virus Res* 244:218–229. <https://doi.org/10.1016/j.virusres.2017.10.014>.
- Baric RS, Crosson S, Damania B, Miller SI, Rubin EJ. 2016. Next-generation high-throughput functional annotation of microbial genomes. *mBio* 7:e01245-16. <https://doi.org/10.1128/mBio.01245-16>.
- U.S. Agency for International Development. 2021. USAID announces new \$125 million project to detect unknown viruses with pandemic potential. Press release.
- Mihara T, Nishimura Y, Shimizu Y, Nishiyama H, Yoshikawa G, Uehara H, Hingamp P, Goto S, Ogata H. 2016. Linking virus genomes with host taxonomy. *Viruses* 8:66. <https://doi.org/10.3390/v8030066>.
- Fu L, Niu B, Zhu Z, Wu S, Li W. 2012. CD-HIT: accelerated for clustering the next-generation sequencing data. *Bioinformatics* 28:3150–3152. <https://doi.org/10.1093/bioinformatics/bts565>.
- Li W, Godzik A. 2006. Cd-hit: a fast program for clustering and comparing large sets of protein or nucleotide sequences. *Bioinformatics* 22:1658–1659. <https://doi.org/10.1093/bioinformatics/btl158>.
- Ashburner M, Ball CA, Blake JA, Botstein D, Butler H, Cherry JM, Davis AP, Dolinski K, Dwight SS, Eppig JT, Harris MA, Hill DP, Issel-Tarver L, Kasarskis A, Lewis S, Matese JC, Richardson JE, Ringwald M, Rubin GM, Sherlock G. 2000. Gene ontology: tool for the unification of biology. The Gene Ontology Consortium. *Nat Genet* 25:25–29. <https://doi.org/10.1038/75556>.
- Gene Ontology Consortium. 2021. The Gene Ontology resource: enriching a GOLD mine. *Nucleic Acids Res* 49:D325–D334. <https://doi.org/10.1093/nar/gkaa1113>.
- Johnson LS, Eddy SR, Portugaly E. 2010. Hidden Markov model speed heuristic and iterative HMM search procedure. *BMC Bioinformatics* 11:431. <https://doi.org/10.1186/1471-2105-11-431>.
- Koch PD, Miller HR, Yu G, Tallarico JA, Sorger PK, Wang Y, Feng Y, Thomas JR, Ross NT, Mitchison T. 2018. A high content screen in macrophages identifies small molecule modulators of STING-IRF3 and NFκB signaling. *ACS Chem Biol* 13:1066–1081. <https://doi.org/10.1021/acscchembio.7b01060>.
- Sun L, Wu J, Du F, Chen X, Chen ZJ. 2013. Cyclic GMP-AMP synthase is a cytosolic DNA sensor that activates the type-I interferon pathway. *Science* 339:786–791. <https://doi.org/10.1126/science.1232458>.
- de Bouteiller O, Merck E, Hasan UA, Hubac S, Benguigui B, Trinchieri G, Bates EEM, Caux C. 2005. Recognition of double-stranded RNA by human Toll-like receptor 3 and downstream receptor signaling requires multimerization and an acidic pH. *J Biol Chem* 280:38133–38145. <https://doi.org/10.1074/jbc.M507163200>.
- Barro M, Patton JT. 2005. Rotavirus nonstructural protein 1 subverts innate immune response by inducing degradation of IFN regulatory factor 3. *Proc Natl Acad Sci U S A* 102:4114–4119. <https://doi.org/10.1073/pnas.0408376102>.

20. Lin Y, Horvath F, Aligo JA, Wilson R, He B. 2005. The role of simian virus 5 V protein on viral RNA synthesis. *Virology* 338:270–280. <https://doi.org/10.1016/j.virol.2005.05.014>.
21. Eaglesham JB, Pan Y, Kupper TS, Kranzusch PJ. 2019. Viral and metazoan poxins are cGAMP-specific nucleases that restrict cGAS-STING signalling. *Nature* 566:259–263. <https://doi.org/10.1038/s41586-019-0928-6>.
22. Shaw ML, Cardenas WB, Zamarin D, Palese P, Basler CF. 2005. Nuclear localization of the Nipah virus W protein allows for inhibition of both virus- and Toll-like receptor 3-triggered signaling pathways. *J Virol* 79:6078–6088. <https://doi.org/10.1128/JVI.79.10.6078-6088.2005>.
23. Wuerth JD, Habjan M, Wulle J, Superti-Furga G, Pichlmair A, Weber F. 2018. NSs protein of sandfly fever Sicilian phlebovirus counteracts interferon (IFN) induction by masking the DNA-binding domain of IFN regulatory factor 3. *J Virol* 92:e01202-18. <https://doi.org/10.1128/JVI.01202-18>.
24. Ning Y-J, Feng K, Min Y-Q, Deng F, Hu Z, Wang H. 2017. Heartland virus NSs protein disrupts host defenses by blocking the TBK1 kinase-IRF3 transcription factor interaction and signaling required for interferon induction. *J Biol Chem* 292:16722–16733. <https://doi.org/10.1074/jbc.M117.805127>.
25. Chen S, Wu Z, Wang M, Cheng A. 2017. Innate immune evasion mediated by Flaviviridae non-structural proteins. *Viruses* 9:291. <https://doi.org/10.3390/v9100291>.
26. Sims AC, Tilton SC, Menachery VD, Gralinski LE, Schäfer A, Matzke MM, Webb-Robertson B-JM, Chang J, Luna ML, Long CE, Shukla AK, Bankhead AR, Burkett SE, Zornetzer G, Tseng C-TK, Metz TO, Pickles R, McWeeney S, Smith RD, Katze MG, Waters KM, Baric RS. 2013. Release of severe acute respiratory syndrome coronavirus nuclear import block enhances host transcription in human lung cells. *J Virol* 87:3885–3902. <https://doi.org/10.1128/JVI.02520-12>.
27. Ng CS, Stobart CC, Luo H. 2021. Innate immune evasion mediated by picornaviral 3C protease: possible lessons for coronaviral 3C-like protease? *Rev Med Virol* 31:e2206. <https://doi.org/10.1002/rmv.2206>.
28. Wang D, Fang L, Wei D, Zhang H, Luo R, Chen H, Li K, Xiao S. 2014. Hepatitis A virus 3C protease cleaves NEMO to impair induction of beta interferon. *J Virol* 88:10252–10258. <https://doi.org/10.1128/JVI.00869-14>.
29. Petersen JM, Her L-S, Dahlberg JE. 2001. Multiple vesiculoviral matrix proteins inhibit both nuclear export and import. *Proc Natl Acad Sci U S A* 98:8590–8595. <https://doi.org/10.1073/pnas.151240998>.
30. Niopek D, Wehler P, Roensch J, Eils R, Di Ventura B. 2016. Optogenetic control of nuclear protein export. *Nat Commun* 7:10624. <https://doi.org/10.1038/ncomms10624>.
31. Niopek D, Benzinger D, Roensch J, Draebing T, Wehler P, Eils R, Di Ventura B. 2014. Engineering light-inducible nuclear localization signals for precise spatiotemporal control of protein dynamics in living cells. *Nat Commun* 5:4404. <https://doi.org/10.1038/ncomms5404>.
32. Yoo TY, Mitchison TJ. 2021. O-GlcNAc modification of nuclear pore complexes accelerates bidirectional transport. *J Cell Biol* 220:e202010141. <https://doi.org/10.1083/jcb.202010141>.
33. Addetia A, Lieberman NAP, Phung Q, Hsiang T-Y, Xie H, Roychoudhury P, Shrestha L, Loprieno MA, Huang M-L, Gale M, Jerome KR, Greninger AL. 2021. SARS-CoV-2 ORF6 disrupts bidirectional nucleocytoplasmic transport through interactions with Rae1 and Nup98. *mBio* 12:e00065-21. <https://doi.org/10.1128/mBio.00065-21>.
34. Kaczorowska J, van der Hoek L. 2020. Human anelloviruses: diverse, omnipresent and commensal members of the virome. *FEMS Microbiol Rev* 44:305–313. <https://doi.org/10.1093/femsre/fuaa007>.
35. Beachboard DC, Horner SM. 2016. Innate immune evasion strategies of DNA and RNA viruses. *Curr Opin Microbiol* 32:113–119. <https://doi.org/10.1016/j.mib.2016.05.015>.
36. Banerjee AK, Blanco MR, Bruce EA, Honson DD, Chen LM, Chow A, Bhat P, Ollikainen N, Quinodoz SA, Loney C, Thai J, Miller ZD, Lin AE, Schmidt MM, Stewart DG, Goldfarb D, De Lorenzo G, Rihn SJ, Voorhees RM, Botten JW, Majumdar D, Guttman M. 2020. SARS-CoV-2 disrupts splicing, translation, and protein trafficking to suppress host defenses. *Cell* 183:1325–1339.E21. <https://doi.org/10.1016/j.cell.2020.10.004>.
37. Hayn M, Hirschenberger M, Koepke L, Nchioua R, Straub JH, Klute S, Hunszinger V, Zech F, Prelli Bozzo C, Aftab W, Christensen MH, Conzelmann C, Müller JA, Srinivasachar Badarinarayan S, Stürzel CM, Forne I, Stenger S, Conzelmann K-K, Münch J, Schmidt FI, Sauter D, Imhof A, Kirchhoff F, Sparrer KMJ. 2021. Systematic functional analysis of SARS-CoV-2 proteins uncovers viral innate immune antagonists and remaining vulnerabilities. *Cell Rep* 35:109126. <https://doi.org/10.1016/j.celrep.2021.109126>.
38. Hale BG, Randall RE, Ortín J, Jackson D. 2008. The multifunctional NS1 protein of influenza A viruses. *J Gen Virol* 89:2359–2376. <https://doi.org/10.1099/vir.0.2008/004606-0>.
39. Mielech AM, Chen Y, Mesecar AD, Baker SC. 2014. Nidovirus papain-like proteases: multifunctional enzymes with protease, deubiquitinating and deISGylating activities. *Virus Res* 194:184–190. <https://doi.org/10.1016/j.virusres.2014.01.025>.
40. Arze CA, Springer S, Dudas G, Patel S, Bhattacharyya A, Swaminathan H, Brugnara C, Delagrave S, Ong T, Kahvejian A, Echelard Y, Weinstein EG, Hajjar RJ, Andersen KG, Yozwiak NL. 2021. Global genome analysis reveals a vast and dynamic anellovirus landscape within the human virome. *Cell Host Microbe* 29:1305–1315.E6. <https://doi.org/10.1016/j.chom.2021.07.001>.
41. Kasuga Y, Zhu B, Jang K-J, Yoo J-S. 2021. Innate immune sensing of coronavirus and viral evasion strategies. *Exp Mol Med* 53:723–736. <https://doi.org/10.1038/s12276-021-00602-1>.